Supplementary information

Revealing the potential crystal structures of the earth-abundant non-toxic photovoltaic $CuBiI_4$

Lan Wang[1#], Yijiang Bao[2#], Shichao Wang[2], Fengchao Wang[2], Congwei Xie[1,3], Keith T. Butler[4*], Xiaoli Fan[1*]*

[1]State Key Laboratory of Solidification Processing, School of Material Science and Engineering, Northwestern Polytechnical University, 127 YouYi Western Road, Xi'an, Shaanxi, 710072, China

[2]Queen Mary University of London Engineering School, Northwestern Polytechnical University, 127 YouYi Western Road, Xi'an, Shaanxi, 710072, China

[3]Skolkovo Institute of Science and Technology, Skolkovo Innovation Center 143026, 3 Nobel Street, Moscow, Russian Federation

[4] Department of Chemistry, University of Reading, Whiteknights, RG6 6AH, UK

* Corresponding authors:

Congwei Xie: Congwei.Xie@skoltech.ru, Keith T. Butler: k.butler@reading.ac.uk and Xiaoli Fan: xlfan@nwpu.edu.cn

Crystal structure prediction

According to the symmetry of the structures, the 15 predicted structures are denoted as $P\bar{1}$, $P\bar{1}$-II, $P\bar{1}$-III, $P\bar{1}$-IV, $P\bar{1}$-V, *P*c, $P2_1/m$, $P2_1/m$-II, $P2_1/m$-III, $P2_1/m$-IV, $P2_1$, $P2/c$, *C*m, *C*c, $P2_12_12$. Table S1 shows the structure names, space groups, number of atoms in the unit cell, volume and formation energy of the 15 $CuBiI_4$ structures. These 15 structures respectively belong to triclinic system ($P\bar{1}$、$P\bar{1}$-II、$P\bar{1}$-III、$P\bar{1}$-IV、$P\bar{1}$-V), monoclinic system (*P*c、$P2_1/m$、$P2_1/m$-II、$P2_1/m$ -III、$P2_1/m$ -IV、$P2_1$、$P2/c$、*C*m、*C*c) and orthorhombic system ($P2_12_12$). The unit cells of *C*m and *C*c structure have 24 atoms, whose v1olumes are 1239 Å^3 and 1049 Å^3, respectively. The unit cells of other structures have 12 atoms (2 Cu atoms, 2 Bi atoms and 8 I atoms), whose volumes are 521 ~ 610 Å^3.

The formation energies are calculated as:

$$E_{form} = (E_{CuBiI_4} - n_{cu}E_{Cu} - n_{Bi}E_{Bi} - n_{Bi}\,E_I)/n_{total} \quad \text{(S1)}$$

where E_{CuBiI_4} is the energy of $CuBiI_4$ unit cell, E_{Cu}, E_{Bi}, E_{I} are the energies of single Cu, Bi, I atoms, respectively, n_{cu}, n_{Bi}, n_I, n_{total} represent the number of Cu, Bi, I atom, and the total number of atoms in the unit cell, respectively. The formation energies of 15 $CuBiI_4$ structures are all negative, indicating that they are all energetical favorable.

Table S1. Structure name, space group, number of atoms per unit cell, volume of the unit cell and formation energy of the 15 predicted $CuBiI_4$ structures.

Structure name	Space group	Number of atoms/unit cell	Volume (Å^3)/unit cell	E^{form} (eV/atoms)
$P\bar{1}$	$P\bar{1}$	12	538.0	-0.355
$P\bar{1}$-II	$P\bar{1}$	12	600.3	-0.340
$P\bar{1}$-III	$P\bar{1}$	12	542.5	-0.311
$P\bar{1}$-IV	$P\bar{1}$	12	523.2	-0.354
$P\bar{1}$-V	$P\bar{1}$	12	573.1	-0.334
*P*c	*P*c	12	526.5	-0.351
$P2_1/m$	$P2_1/m$	12	521.2	-0.338
$P2_1/m$-II	$P2_1/m$	12	585.8	-0.341
$P2_1/m$-III	$P2_1/m$	12	610.0	-0.341
$P2_1/m$-IV	$P2_1/m$	12	575.2	-0.331
$P2_1$	$P2_1$	12	521.2	-0.351
*P*2/*c*	*P*2/*c*	12	524.6	-0.323
*C*m	*C*m	24	1238.6	-0.327
*C*c	*C*c	24	1049.2	-0.328
$P2_12_12$	$P2_12_12$	12	532.4	-0.315

Dynamical and mechanical stability analysis

The phonon dispersion spectrum of the 15 structures along the high symmetry directions are shown in Figure S1. Among the 15 structures, the phonon spectra of $P\bar{1}$ - II, $P\bar{1}$ - III and $P2_1/m$ structures have no imaginary frequencies, indicating their dynamical stability. Except for $P\bar{1}$ - II, $P\bar{1}$ - III and $P2_1/m$ structures, the phonon spectra of other structures all have imaginary frequencies.

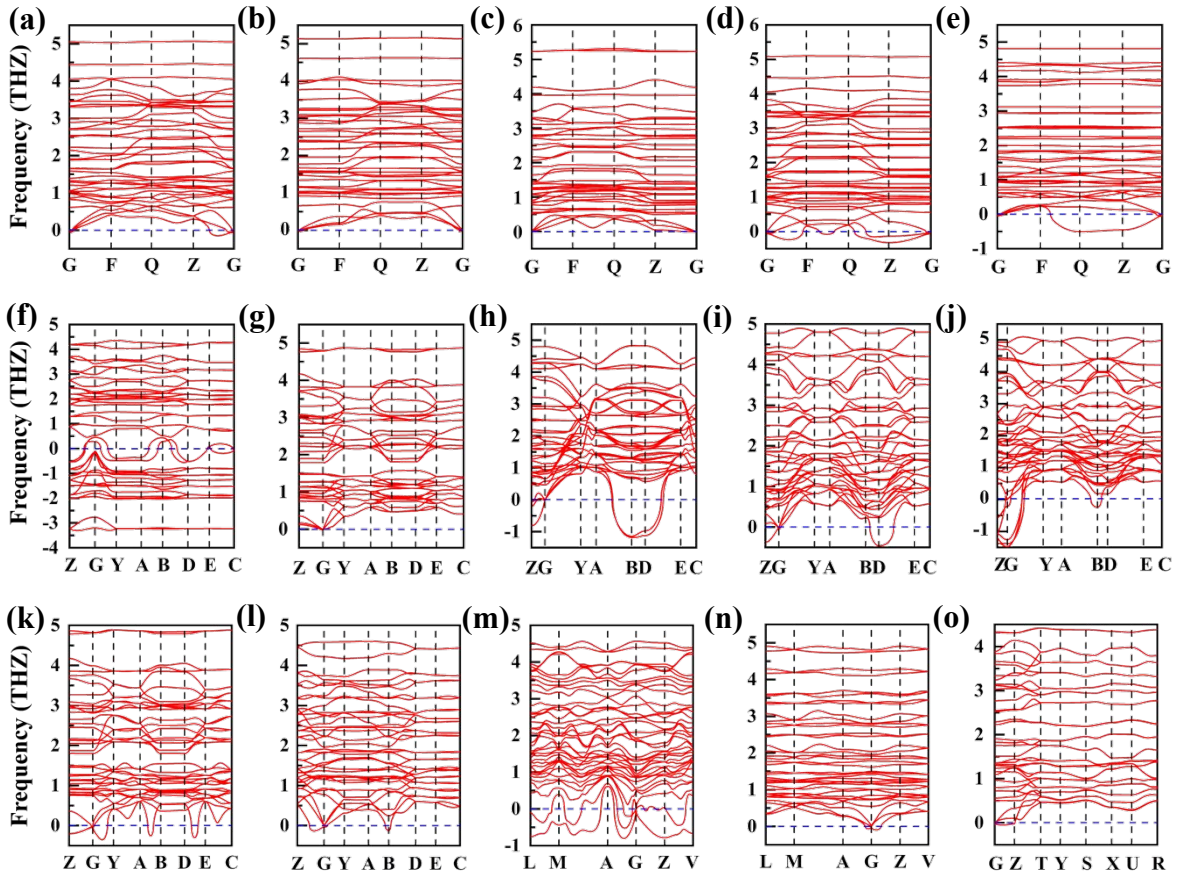

Figure S1. Phonon dispersion spectra of the 15 predicted $CuBiI_4$ structures. (a) $P\bar{1}$, (b) $P\bar{1}$-II, (c) $P\bar{1}$-III, (d) $P\bar{1}$-IV, (e) $P\bar{1}$-V, (f) *P*c, (g) $P2_1/m$, (h) $P2_1/m$-II, (i) $P2_1/m$-III, (j) $P2_1/m$-IV, (k) $P2_1$, (l) $P2/c$, (m) *C*m, (n) *C*c, (o) $P2_12_12$.

The elastic constants of the $P\bar{1}$ - II, $P\bar{1}$ - III and $P2_1/m$ structures were also calculated and are shown in Table S2. There are 21 independent elastic constants for triclinic structure, the positive definiteness of all the elastic constants ensures the mechanical stability. The monoclinic structure has 13 independent elastic constants, and the mechanical stability should be judged according to the Born-Huang criteria. [1, 2] $P\bar{1}$ - II, $P\bar{1}$ - III and $P2_1/m$ all satisfy the Born-Huang criteria, which indicates that they are mechanical stable.

Table S2. Calculated elastic constants for the three $CuBiI_4$ structures ($P\bar{1}$-II, $P\bar{1}$-III, $P2_1/m$).

C_{ij} (GPa)	$P\bar{1}$-II	$P\bar{1}$-III	$P2_1/m$
C_{11}	19.8	13.3	20.7
C_{22}	3.3	20.0	18.9
C_{33}	14.0	3.1	3.7
C_{44}	3.9	1.2	1.4
C_{55}	5.1	0.8	1.7
C_{66}	1.8	9.0	7.8
C_{12}	1.3	6.9	4.5
C_{13}	4.0	0.1	0.2
C_{14}	1.3	-0.2	—
C_{15}	-0.9	-0.2	-0.2
C_{16}	-1.3	-0.7	—
C_{23}	3.3	0.4	1.4
C_{24}	1.1	-0.6	—
C_{25}	0.8	0.1	-0.4
C_{26}	-0.6	-4.5	—
C_{34}	4.5	0.2	—
C_{35}	1.4	0.3	0.2
C_{36}	-0.5	0.1	—
C_{45}	0.1	0.1	—
C_{46}	-0.1	0.6	-0.2
C_{56}	1.9	-0.1	—

Crystal structures analysis

As shown in Figure 1(a) in the main text, the $P\bar{1}$ - II structure is classified into triclinic crystal system, with lattice constants of a = 7.5 Å, b = c = 8.9 Å. The bond lengths of Cu-I and Bi-I are 2.6 ~ 2.7 Å and 3.1 ~ 3.2 Å, respectively, as listed in Tble S3. The structure is layered in the [010] direction, each layer is composed of the octahedra BiI_6 and tetrahedra CuI_4 via sharing edges; along [001] direction, the octahedra BiI_6 are connected by the common edges; along [100] direction, the octahedra BiI_6 is connected by two tetrahedra CuI_4 via sharing edges to a layered structure.

Table S3. The lattice constants and Cu/Bi-I bond length of the three $CuBiI_4$ structures ($P\bar{1}$-II, $P\bar{1}$-III, $P2_1/m$).

Structure name	a (Å)	b (Å)	c (Å)	α (°)	β (°)	γ (°)	Cu-I (Å)	Bi-I (Å)
$P\bar{1}$-II	7.5	8.9	8.9	61.6	88.1	85.8	2.6 ~ 2.7	3.1 ~ 3.2
$P\bar{1}$-III	7.2	8.9	9.0	104.6	98.9	92.7	2.6 ~ 2.8	3.1 ~ 3.2
$P2_1/m$	7.0	9.0	8.0	90.0	90.5	90.0	2.6 ~ 2.7	3.1 ~ 3.2

As shown in Figure 1(b) in the main text, the $P\bar{1}$ - III structure belongs to the triclinic crystal system, with lattice constants a = 7.2 Å, b = 8.9 Å, c = 9.0 Å. The bond lengths of Cu-I and Bi-I are 2.6 ~ 2.8 Å and 3.1 ~ 3.2 Å, respectively, as listed in Tble S3. Similar to $\bar{P}1$-II, $P\bar{1}$ - III is also a layered structure, and has CuI_4 tetrahedra and BiI_6 octahedra. But the tetrahedra CuI_4 and octahedra BiI_6 arrange differently: the octahedra BiI_6 is connected with each other via

sharing vertices; the tetrahedra CuI_4 is embedded on octahedra BiI_6 via sharing faces or edges. The Bi atoms are located on the center of the a and b edges.

Figure 1(c) in the main text shows the $P2_1/m$ structure. The $P2_1/m$ structure is a monoclinic crystal with lattice constants a = 7.0 Å, b = 9.0 Å, c = 8.0 Å. Bi atoms occupy the vertex position of the unit cell and the center of the edges in the [010] direction. The Cu-I bond lengths are 2.6 ~ 2.7 Å, and Bi-I bond lengths are 3.1 ~ 3.2 Å, as listed in Tble S3. The $P2_1/m$ structure is a layered structure. Along [010] direction, the octahedra BiI_6 forms a chain by sharing edges and connects to two tetrahedra CuI_4; the tetrahedra CuI_4 does not contact with each other.

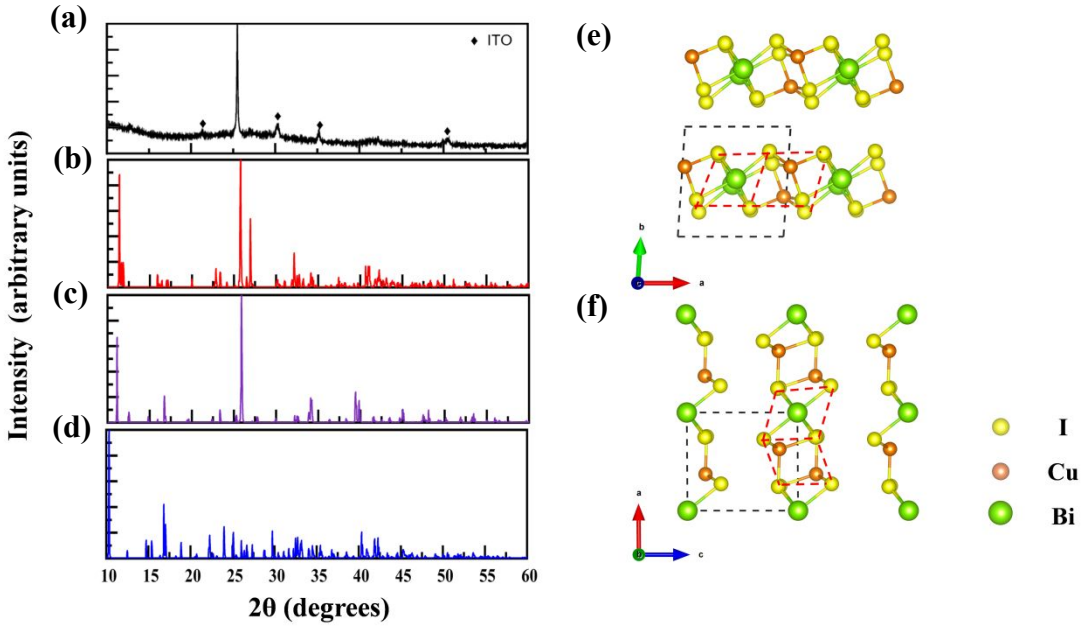

Figure S2. (a) The experimental XRD data for $CuBiI_4$ [3], and our simulated XRD for the three $CuBiI_4$ structures of (b) $P\bar{1}$-II, (c) $P2_1$/m, (d) $P\bar{1}$-III. The atomic arrangement of (e) $P\bar{1}$-II, (f) $P2_1/m$.

The XRD spectra of the three $CuBiI_4$ structures are further simulated, and the simulation results are shown in Figure S2(b-d). Figure S2(a) shows the previously reported experimental XRD spectrum. There is a strong diffraction peak locating at 25.50°, and three tiny diffraction peaks locating at about 12.72°, 42.23° and 50.02°, respectively. [3] It shows that the peak position

and peak intensity in the XRD spectrum of the $P2_1/m$ are consistent with the experimental data. The first peak position of $P2_1/m$ slightly deviates from the experimental results, and the positions and intensities of other peaks agree with the experimental results. We also found that $P\bar{1}$-II is similar to $P2_1/m$ except for an additional peak at 25.50°. The commonality of the two structures can be explained from the arrangement of atoms (Figure S2(e-f)): I atoms present a layered arrangement, locating on both sides of Bi/Cu atoms; Bi atoms and I atoms form the octahedron BiI_6; Cu atoms locate in two positions, the center of two adjacent tetrahedral CuI_4 with shared edges; both structures are layered structures formed by alternately connecting octahedron BiI_6 and shared-edge tetrahedron CuI_4. In addition, we infer that the peak of $P\bar{1}$-II at 25.50°, which is different from the $P2_1/m$, originates from the twisted layered arrangement of I atoms. These structural features illustrate the crystal structure of experimentally synthesized $CuBiI_4$ in a certain extent [3]. The peak positions and peak intensities in the XRD spectrum of $P\bar{1}$ - III structure are quite different from the experimental data, which is a new unreported $CuBiI_4$ crystal structure.

Electronic properties analysis

Table S4. Band gaps (E_g) calculated by the HSE06 method, positions of VBM and CBM, Bader charge of the three $CuBiI_4$ structures ($P\bar{1}$-II, $P\bar{1}$-III, $P2_1/m$).

Structure name	E_g (eV)	VBM	CBM	Bader charge		
				Cu (e/atom)	Bi (e/atom)	I (e/atom)
$P\bar{1}$-II	2.0	0 0 0	0 0 0	0.31	1.09	-0.35
$P\bar{1}$-III	1.4	0 0 0	0 0 0.5	0.32	1.04	-0.34
$P2_1/m$	1.9	0 0 0.44	0 0 0	0.32	1.08	-0.35

The electronic band structures of the three $CuBiI_4$ structures were calculated by the PBE and HSE06 methods. Comparing the results shown in Figure 3 in the main text calculated by the HSE06 and PBE methods, the conduction/valence bands calculated by the HSE06 method move upwards/downwards. Correspondingly, the band gaps calculated by the HSE06 method are larger. Except that, the profile of the band structures calculated by the two methods are similar with each other. As shown in Figure 2 in the main text, the Valence Band Maximum (VBM) is mainly contributed by the Cu-3*d* orbital and the I-5*p* orbital, showing the feature of Cu-I covalent bond. The Conduction Band Minimum (CBM) mainly attributes to the Bi-6*p* and I-5*p* orbitals.

The $P\bar{1}$-II structure is a direct band gap semiconductor, with the VBM and CBM locating at G point; its band gap is 2.0 eV. $P\bar{1}$ - III and $P2_1/m$ behave as indirect band gap semiconductors; the positions of their VBM and CBM are shown in Table S4. The band gap of $P\bar{1}$ - III is 1.4 eV,

which is the best band gap (1.4 eV) for the absorber materials in solar cell applications. The band gap of $P2_1/m$ is 1.9 eV, within the energy range of visible light (1.64 ~ 3.19 eV). The appropriate direct band gap tends to have better light adsorption properties. [4] In contrast, the electron transition in the indirect band gap semiconductor involves the participation of phonons, and the radiative transition probability of indirect band gap semiconductor is much smaller than that of direct band gap semiconductor.

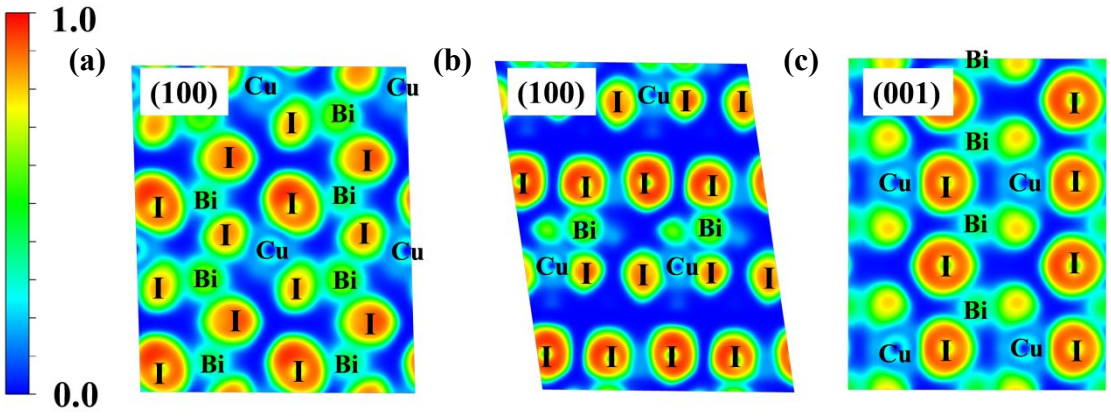

Figure S3. Electronic local function (ELF) for the three $CuBiI_4$ structures. (a) $P\bar{1}$-II on (100) plane, (b) $P\bar{1}$-III on (100) plane, (c) $P2_1/m$ on (001) plane.

The Electronic Localization Function (ELF) plays a significant role in understanding the bond character and the distribution of valence electrons. We further calculated the ELF for the three $CuBiI_4$ structures. Figure S3 shows the ELF on the (100) planes of $P\bar{1}$-II, (100) planes of $P\bar{1}$-III, (001) planes of $P2_1/m$. The ELF values near the I atoms are close to 1, indicating highly localized electron distribution. The ELF values near the Bi atoms are close to 0.5, and the corresponding electron distribution can be regarded as the boundary between the localized distribution and the delocalized distribution, where the electrons form a homogeneous electron gas distribution. The ELF value near Cu atoms are close to 0.2, indicating the electrons delocalization. Among the three $CuBiI_4$ structures, the corresponding ELF value between the

Cu/Bi atom and the I atom is only about 0.2, indicating the strong ionic and weak covalent of Cu/Bi-I bond.

We adopted the Bader charge analysis to study the electron transfer between Cu, Bi and I atoms. The results are summarized in Table S4. It shows that the Cu and Bi atoms lose ~ 0.32e and 1.04 ~ 1.08e electrons, respectively; I atoms gain 0.34 ~ 0.35e electrons. The results indicate great derivation from the feature of the pure ionic bond interaction, which proves that there are not only ionic bonds but also covalent bonds between Cu/Bi atoms and I atoms. The covalent interaction of Cu/Bi-I can also be confirmed by PDOS in Figure 2 in the main text, there are obvious hybridization between Cu-3*d*, Bi-6*p* orbitals and I-5*p* orbitals. Therefore, the Cu-I and Bi-I bonds in the three $CuBiI_4$ structure combine strong ionic with weak covalent, which is similar with the Pb-I bond in $MAPbI_3$. [5]

Light absorption properties analysis

The dielectric function ε (ω) is usually used to describe the linear response to electromagnetic radiation. It includes two parts

$$\varepsilon\ (\omega)\ = \varepsilon_1(\omega) + i\varepsilon_2(\omega) \tag{S2}$$

where $\varepsilon_1(\omega)$ and $\varepsilon_2(\omega)$ represent the real and imaginary parts of the dielectric function, respectively. The imaginary part $\varepsilon_2(\omega)$ is the sum of all the possible transitions from the valence band to the conduction band, which can be calculated as

$$\varepsilon_2(\omega) = \frac{2e^2\pi}{\Omega\varepsilon_0}\sum_{k,v,c}\left|\langle\psi_k^c\left|\,\hat{u}r\,\right|\psi_k^v\rangle\right|^2\delta\left(E_k^c - E_k^v - \mathrm{E}\right) \tag{S3}$$

where e is the electron charge, Ω is the volume of primitive unit cell, ε_0 is the vacuum permittivity, k is the wave vector, the indices c and v denote conduction and valence band states, respectively. $\hat{u}$ is the polarization vector of the incident electric field, r is the position vector of electron, E_k^c/E_k^v and ψ_k^c/ψ_k^v are the eigenvalues and wave functions of the conduction/valence states of c/v, respectively. E is the photon energy, ω is the frequency of incident light, δ is Kronecker delta. The real part $\varepsilon_1(\omega)$ is calculated by Kramers-Kronig transformation:

$$\varepsilon_1(\omega) = 1 + \frac{2}{\pi}P\int_0^\infty \frac{\omega'\varepsilon_2(\omega')}{\omega'^2 - \omega^2}d\omega' \tag{S4}$$

where P is the principle value of integral. The absorption coefficient $I(\omega)$ is calculated as:

$$\mathrm{I}(\omega) = \sqrt{2}\omega\left[\sqrt{\varepsilon_1(\omega)^2 + \varepsilon_2(\omega)^2} - \varepsilon_1(\omega)\right]^{1/2} \quad \text{(S5)}$$

Figure S4(a-c) display the dielectric functions of the three $CuBiI_4$ structures. The imaginary part of the dielectric function, $\varepsilon_2(\omega)$, provides the information about the absorption behavior. The threshold (E_0) of $\varepsilon_2(\omega)$ for $P\bar{1}$ - II, $P\bar{1}$ - III, $P2_1/m$ are 1.9, 1.4, 1.9 eV, respectively, corresponding to their band gaps. There are three main transition peaks for $P\bar{1}$ - II/$P\bar{1}$ - III /$P2_1/m$, which locate at 4.08/3.36/4.06 eV (A1/B1/C1), 4.67/4.60/5.16 eV(A2/B2/C2), 8.14/8.13/8.09 eV (A3/B3/C3), respectively. According to the PDOS shown in Figure 2 in the main text, A1/B1/C1 peaks mainly attribute to the electronic transition from Cu-3*d* state to Bi-6*p* state and I-5*p* state; A2/B2/C2 peak corresponds to the electronic transition from I-5*p* state to Bi-6*p* state; A3/B3/C3 peak mainly corresponds to the electronic transition from Bi-6*p* state to I-5*p* state. The real part $\varepsilon_1(\omega)$ at zero frequency corresponds to the static dielectric constant $\varepsilon_1(0)$. The static dielectric constant $\varepsilon_1(0)$ of $P\bar{1}$ - II/$P\bar{1}$ - III/$P2_1/m$ structure is 5.15/5.61/5.26 eV, which reversely correlate with their band gaps. This can be explained by relationship of $\varepsilon_1(0) \approx 1+(\hbar\omega_p/E_g)^2$. In the photon energy range of 0 ~ 10 eV, $\varepsilon_1(\omega)$ of the three $CuBiI_4$ increases to the maximum value with the increase of photon energy, and then rapidly decreases to the minimum value with the increase of photon energy. After that, with the increase of photon energy, it firstly increases and then decrease with a relatively small amplitude.

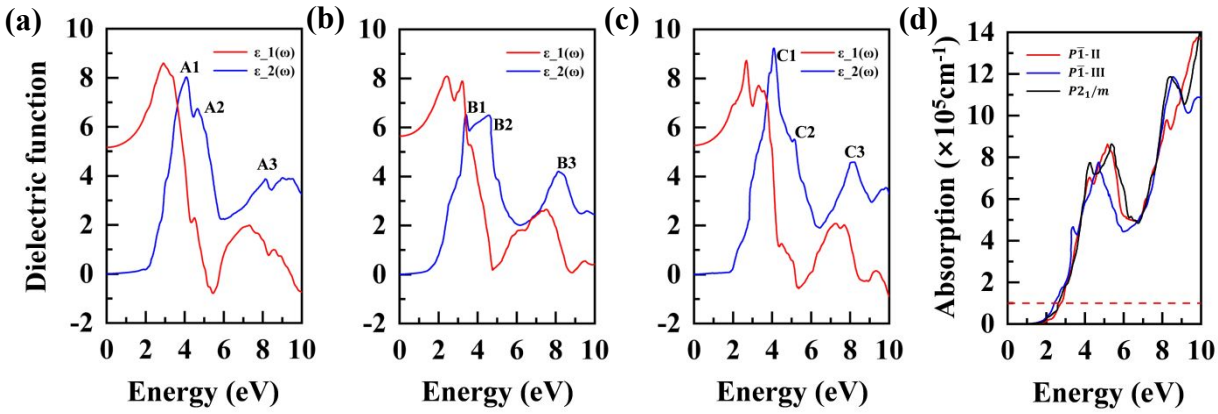

Figure S4. Dielectric function for the three $CuBiI_4$ structures. (a) $P\bar{1}$-II , (b) $P\bar{1}$-III, (c) $P2_1/m$. (d) Optical absorption spectrum of the three $CuBiI_4$ structures. A1/B1/C1, A2/B2/C2, A3/B3/C3 represents the three main peaks of $P\bar{1}$ - II/$P\bar{1}$ - III/$P2_1/m$.

The absorption coefficients of the three $CuBiI_4$ structures are calculated and the absorption spectra are plotted in Figure S4(d). There are three peaks within 0 ~ 10 eV in the adsorption spectrum, whose positions are consistent with the three peaks of $\varepsilon_2(\omega)$ curve. As showing in Figure S4(d), the three $CuBiI_4$ structures start light absorption at 1.90/1.40/2.00 eV, respectively. The absorption intensity increases as the energy increases. It is remarkable that the three $CuBiI_4$ structures all exhibits good absorption in the visible-light region of solar energy with the maximum absorption coefficient all exceeding 1×10^5 cm^{-1}, slightly smaller than that of $MAPbI_3$. [6] Among the three structures, the light absorption of $P\bar{1}$-III is slightly better than that of $P\bar{1}$-II and $P2_1/m$ in the visible light region.

A list of some well matched semiconductors

Table S5. The well matched semiconductors for electron and hole extraction of the three $CuBiI_4$ structures ($P\bar{1}$-II, $P\bar{1}$-III, $P2_1/m$).

Structure name	ETL	HTL
$P\bar{1}$-II	'CdS', 'GaN', 'GaP', 'SnS_2', 'ZnO', 'In_2O_3', 'TiO_2', '$SrTiO_3$', 'Sb_2O_3', '$BaTiO_3$', 'Nb_2O_5', 'PbO', 'CoO', '$CuTiO_3$', 'FeO', '$ZnTiO_3$', 'ZnS_2'	'SrTe', 'WO_3', 'Zn_2TiO_4', 'Gd_2S_3', 'La_2S_3', 'MnS', '$Zn_3In_2S_6$'
$P\bar{1}$-III	'SnO_2'	'Zn_2TiO_4', '$KNbO_3$'
$P2_1/m$	'CdS', 'Fe_2O_3', 'Bi_2O_3', '$CdFe_2O_4$', '$FeTiO_3$', 'PbO', '$YFeO_3$', '$CoTiO_3$', '$NiTiO_3$'	'Zn_2TiO_4', '$Zn_3In_2S_6$'

References

(1) Wu, Z. J.; Zhao, E. J.; Xiang, H. P.; Hao, X. F.; Liu, X. J.; Meng, J. Crystal Structures and Elastic Properties of Superhard IrN_2 and IrN_3 from First Principles. *Phys. Rev. B.* **2007**, *76*, 054115.

(2) Félix, M.; Coudert, F. X. Necessary and Sufficient Elastic Stability Conditions in Various Crystal Systems. *Phys. Rev. B.* **2014**, *90*, 224104.

(3) Zhang, B. S.; Lei, Y.; Qi, R. J.; Yu, H. L.; Yang, X. G.; Cai, T.; Zheng, Z. An In-Situ Room Temperature Route to $CuBiI_4$ Based Bulk-Heterojunction Perovskite-Like Solar Cells. *Sci. China Mater.* **2019**, *62*, 519-526.

(4) Yun, S. N.; Zhou, X.; Even, J.; Hagfeldt, A. Theoretical Treatment of $CH_3NH_3PbI_3$ Perovskite Solar Cells. *Angew. Chem. Int. Edit.* **2017**, *56*, 15806-15817.

(5) Feng, X. X.; Liu, B.; Long, M. Q.; Cai, M.; Peng, Y. Y.; Yang J. L. Improving Stability of Lead Halide Perovskite via PbF_2 Layer Covering. *J. Phys. Chem. Lett.* **2020**, *11*, 6266-6272.

(6) Zhang, Z.; Liu, D. W.; Wu, K. C. First-Principles Study of Structural Stability, Electronic and Optical Properties of GA-Doped $MAPbI_3$. *Spectrochim Acta A.* **2020**, *226*, 117638.